Serb. Astron. J. № 170 (2005), 47 - 56 **UDC 524.354–735–77**
Original scientific paper

A RADIO-CONTINUUM STUDY OF THE SUPERNOVA REMNANT MSH 11–61A

M. D. Filipović[1], J. L. Payne[2] and P. A. Jones[3]

[1] *University of Western Sydney, Locked Bag 1797, Penrith South DC NSW 1797, Australia*

[2] *Centre for Astronomy, James Cook University, Townsville QLD 4811, Australia*

[3] *Australia Telescope National Facility, CSIRO, P.O. Box 76, Epping NSW 1710, Australia*

(Received: March 15, 2005; Accepted: April 10, 2005)

SUMMARY: We present a high-resolution radio-continuum study of Galactic supernova remnant MSH 11–61A. We combine moderate resolution X-ray, radio-continuum and CO data to study the morphology and kinematics of MSH 11–61A. We estimate the radio-continuum spectral index to be $\alpha_{843-4850}$=–0.33±0.07 based on our flux density measurements and also note that this SNR has significant 'turn-over' spectra at lower (29.9-843 MHz) frequencies. The diameter of MSH 11–61A is estimated to be 12.5′ with 'ear' extensions of 4′ to the northwest and southeast. The striking anticorrelation between X-ray and radio-continuum images confirms a mixed-morphology classification of this remnant. The CO images are consistent with a distance reported by Rosado et al. (1996) of about 7 kpc.

Key words. ISM: individual objects: (MSH 11-61A, G290.1-0.8) – ISM: supernova remnants – radio continuum: ISM

1. INTRODUCTION

Since the initial identification of MSH 11–61A by Kesteven (1968), its morphology has been rather confusing because of differing emission between radio and X-rays. It has been classified as both a shell and a radio-filled SNR. Rho and Petre (1998) have probably classified it best as a 'new' prototypical mixed-morphology remnant, shell-like in the radio and centrally filled in the X-ray with little or no limb brightening. Milne et al. (1989) describe MSH 11–61A in the MOST image as consisting of a thick shell with two ear-like extensions towards the northwest and the southeast which are also prominent in the *Einstein* X-ray image. They obtained 8.4 GHz polarization images of the SNR and compared them with earlier 5 GHz polarization observations by Milne and Dickel (1975). Both showed a sudden change in the polarization direction where MSH 11–61A sweeps northwards into the northwest 'ear'. Some of the most prominent properties about this object are given in Table 1.

Milne et al. (1989) also found projected magnetic field directions were difficult to interpret on either a radial or tangential model. With their estimated age of 2.2 kyr, a comparison with similar aged remnants suggested that MSH 11–61A was in a (long) transition phase from radial to tangential fields. Their Faraday rotation measure was positive over most of the remnant with high values in the south and low or negative values in the north.

In the radio-continuum, various flux density measurements for MSH 11–61A are listed in Table 2. Spectral index (α) estimates based on these values are found in the literature and are listed in Table 1.

Kaspi et al. (1997) reported the discovery of a 63 ms radio pulsar, PSR J1105–6107,

at position RA(J2000)=$11^{\rm h}05^{\rm m}26.07^{\rm s}$ and DEC(J2000)=–61°07′52.1″ (well outside of the images in this paper) with a characteristic age of 63 kyr ($\rm P/2\dot{P}$). Dispersion measures revealed this object to be about 7 kpc from the Sun. The spin-down luminosity of this pulsar was 2.5 $\times 10^{36}$ ergs $\rm s^{-1}$, which is in the top 1% of spin-down luminosities and most likely associated with the *CGRO/EGRET* source 3EG J1103–6106. They argue that, although by no means certain, the distance and age of MSH 11–61A could be consistent with an association. In fact, MSH 11–61A has a central X-ray emission which is thermal (see below) supporting the case that it does not contain a central neutron star. A measurement of the pulsar's proper motion, which should be about 22 mas $\rm yr^{-1}$ if the association is real, is needed but may not yet be forthcoming due to the pulsar's timing noise and low flux density.

Optical counterparts of MSH 11–61A were found by Kirshner and Winkler (1979) using the CTIO Curtis Schmidt 4–meter telescope with a combination of Hα (656.5 nm), N II and [S II] (672.5 nm) interference filters. A diffuse ring in the [S II] image was noted corresponding to a superimposed 8.8 GHz map from Dickel et al. (1973). Elliott and Malin (1979) obtained an image of MSH 11–61A in the [S II] band (671.7 and 673.1 nm) at the prime focus of the 3.9-m Anglo-Australian Telescope. They found the Hα/[S II] ratio of 2.1 in MSH 11–61A consistent with old SNRs such as Monoceros and HB9. The high Hα/[S II] ratio of 12.8 from MSH 11–61B was more characteristic of a H II region.

Using data from the *Einstein* Observatory (HEAO2), Seward (1990) reported the detection of MSH 11–61A with *Einstein's* Imaging Proportional Counter (IPC), High Resolution Imager (HRI) and Monitor Proportional Counter (MPC). He noted count rates (counts $\rm s^{-1}$) of 0.47 ± 0.1, 0.13 ± 0.03 and 0.92 ± 0.05, respectively. In the IPC's energy range of 0.3 to 4.5 keV and its resolution of 1′, X-ray energies peaked in the center of the 10.9 ksec image in clear contrast to MSH 11–61A's radio emission. MSH 11–61A was also observed with the *ASCA* (Advanced Satellite for Cosmology and Astrophysics) observatory in 1994 and 1995 as reported by Slane et al. (2002). They merged data to form a GIS (Gas Imaging Spectrometer) and a SIS (Solid-state Imaging Spectrometer, the first X-ray CCD) spectrum in the 0.5–10 keV range and found the X-ray emission to be of thermal origin.

Two mechanisms for this thermal X-ray emission were investigated by Slane et al. (2002). The Cloudy ISM model (Cowie and McKee 1977) involves a two-phase ISM containing cold clouds embedded in a warmer diffuse intercloud medium. The blast wave rapidly passes cold clouds, leaving them intact in the hot postshock gas. White and Long (1991) developed a similarity solution for this in which the cold clouds slowly evaporate, increasing the SNR's central X-ray emission. A second proposed mechanism, thermal conduction, occurs later in a SNR's evolution. In this model, the shock front slows, becoming radiative as the shocked material cools immediately. With this idea in mind, Cox et al. (1999) modeled SNR W44 using thermal conduction via Coloumb collisions between the electrons and ions inside the hot plasma.

Table 1. Known properties of MSH 11–61A.

Description	*Value*
RA/Dec (J2000)	$11^{\rm h}03^{\rm m}$, –60°54′
Galactic	l=290.1°, b=-0.8°
Other Name	G290.1–0.8
Type	"S" shell type, Green (2001)
	"F" radio-filled, Seward (1990)
	Mixed, Rho and Petre (1998)
Dimensions	14′× 10′, Slane et al. (2002)
	19′× 14′, Whiteoak and Green (1996)
	12′, Dickel et al. (1973)
	12.4′× 11.4′, Shaver and Goss (1970)
	31 pc, Rosado et al. (1996)
	40–50 pc, 15′, Elliott and Malin (1979)
	14 pc, Kirshner and Winkler (1979)
	21.1 pc, Clark and Caswell (1976)
Distance	8–11 kpc, Slane et al. (2002)
	6.9 kpc, Rosado et al. (1996)
	12–14 kpc, Elliott and Malin (1979)
	5.8 kpc, Clark and Caswell (1976)
	3.4–4 kpc, Dickel (1973)
Age	10–20 kyr, Slane et al. (2002)
	2.2 kyr, Milne et al. (1989)
	2.5 kyr, Clark and Caswell (1976)
Association	PSR J1105–6107, Kaspi et al. (1997)
Spectral Index	-0.43 ± 0.8, Milne et al. (1989)
	-0.55, Clark and Caswell (1976)
	-0.62, Dickel et al. (1973)

Table 2. Radio-continuum flux densities.

Frequency (MHz)	*FluxDensity* (Jy)	*Reference*
29.9	35±7	Jones and Finlay (1974)
408	99.1	Shaver and Goss (1970)
843	43±10%	Whiteoak and Green (1996)
843	45±11	Milne et al. (1989)
5000	20.2	Milne and Dickel (1975)
8400	19.5±1.0	Milne et al. (1989)
8800	18.4	Dickel et al. (1973)

Slane et al. (2002) attempted to reproduce the observed center-filled X-ray properties of MSH 11–61A and derive associated age, energy and ambient density conditions implied by each model. In general, the Cloudy ISM Model was favored in comparisons with observed X-ray surface brightness and temperature profiles. They estimated explosion energies for the associated supernova in the range of $(0.5 - 1) \times 10^{51}$ ergs. Using either model to determine the necessary velocity of PSR J1105–6107, Slane et al. (2002) found a range of $(4.5 - 5.3) \times 10^3$ km s^{-1} and suggested that an association with MSH 11–61A was not likely.

Studying kinematics of this SNR, Rosado et al. (1996) claim MSH 11–61A to be in a zone where several background and foreground nebulae at different velocities are seen in projection. They made use of a scanning Fabry-Perot interferometer to survey the Hα line of the SNR and analyzed the results along with similar galactic survey data. Radial velocity profiles (each covering 20 × 20 pixel 'windows') were found to fit very complicated motions within the field. For example, the N-filament seen in Elliott and Malin (1979) was detected at negative velocities where it seemed to belong to the large diameter arc towards the northeast region of the field. This suggested that most of this emission was due to the arc and that the SNR contributed only a small amount.

In fact, good fits to the SNR and surrounding H II regions were made using two velocity components. Their interpretation was that there are two sets of H II regions, superimposed in projection. Regions at –20 km s^{-1} implied a distance of 2.9 kpc while regions at +20 km s^{-1} implied a distance of greater than 8 kpc. Thus, they felt they were seeing two different regions of a spiral arm with the SNR (+9 to +15 km s^{-1}) somewhere in between. Using subtraction methods, they determined that the systemic radial velocity of MSH 11–61A was about +12 km s^{-1} corresponding to a distance of 6.9 kpc.

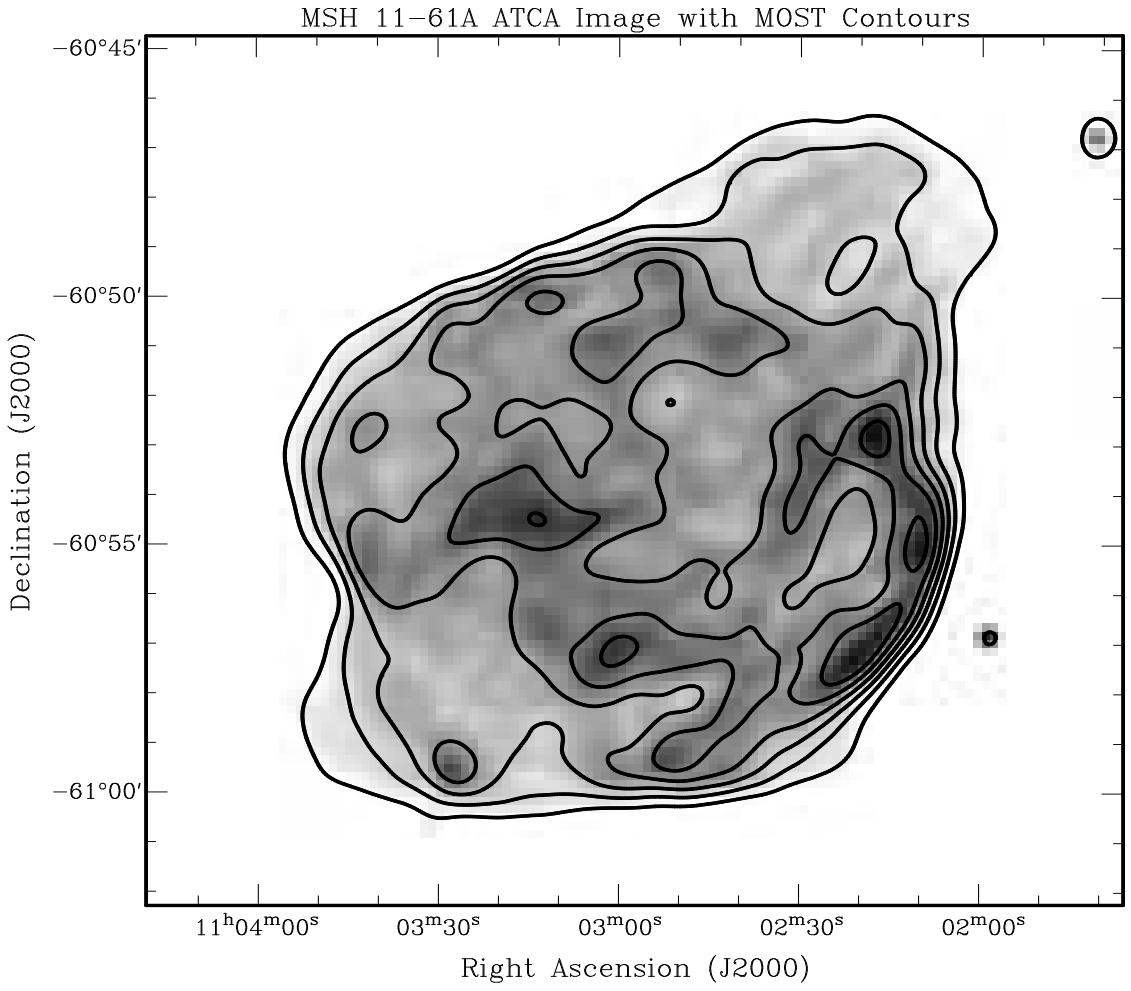

Fig. 1. *The ATCA 21.8 cm radio-continuum image (primary beam corrected) of MSH 11–61A overlaid with MOST (843 MHz) contours at 0.05, 0.10, 0.15, 0.20, 0.25 and 0.30 Jy beam^{-1}. The ATCA image resolution is 21″ and the MOST beam is 49″ × 43″.*

In this paper we present our new radio and CO observations of MSH 11–61A. We also re-examined 843 MHz (MOST) and 4850 MHz (PMN) images of MSH 11–61A allowing the calculation of a new radio spectral index. We show the resulting radio spectrum plot suggesting MSH 11–61A's non-thermal nature in the radio domain with a turn-over of the spectral index at mid to low frequencies. Finally, comparisons between our ATCA and NANTEN images with archival *ROSAT* images help to clarify previous confusion about the morphology of MSH 11–61A.

2. DATA

2.1 Radio-Continuum

In 1995, we made two 12 hour synthesis observations with the ATCA in the 1.5C-km (16 May) and 750C-m configurations (1 June), using two 128 MHz bands (14×8 MHz channels) centered on a frequency of 1378 MHz (Table 3). The pointing center was set to RA(J2000)=$11^{\rm h}03^{\rm m}22.6^{\rm s}$ and DEC(J2000)=–60°56′51.0″. The resulting ∼21′ radius primary beam corrected 1378 MHz (λ=21.8 cm) radio image (see Fig. 1) was well matched to the area covered by the *ROSAT* image (described below). All observations were completed at night when solar interference was minimal and wind conditions were more stable, allowing the single dish pointing accuracy to be as high as possible.

Calibration and editing was completed in the MIRIAD data reduction package at the ATNF, based on standard procedures developed by Sault and Killeen (2003). The source 1934-638 was used as the primary calibrator and 1036-697 as the secondary calibrator. The calibrated data was then imaged (256×256, 10″ pixels) and cleaned (∼450 000 iterations). The cleaned images reached an rms of 2.5 mJy. After combining both observations (configurations) the final image resolution was set to 21″× 21″.

We have also re-examined 843 MHz and 4850 MHz images of MSH 11–61A. In the MOST (Molonglo Observatory Synthesis Telescope) survey, 70′× 70′ cosec(δ) areas of the sky were observed over a 12 hour period at 843 MHz. Detailed information about this study may be found in Whiteoak and Green (1996).

The PARKES-MIT-NRAO (PMN) survey produced a 4850 MHz image of MSH 11–61A using the Parkes 64-meter radio telescope during its June 1990 session (Griffith and White 1993; Wright et al. 1994). The 4.4 σ flux limit for this Southern Survey was about 32 mJy at –60° declination.

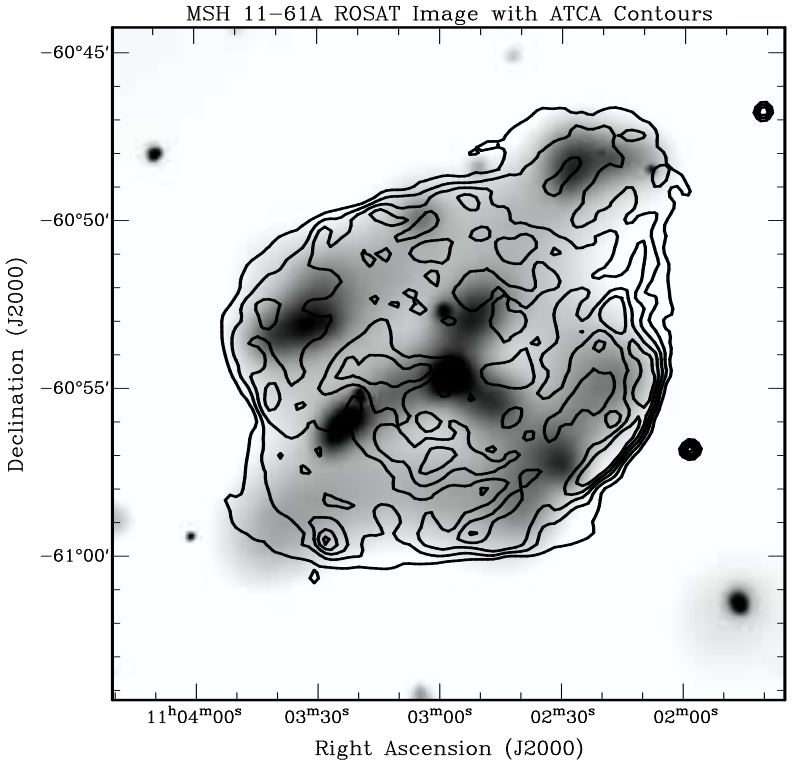

Fig. 2. *The ROSAT HRI image (range 2–8 counts) of MSH 11–61A overlaid with ATCA contours at 0.01, 0.02, 0.03, 0.04 and 0.05 Jy beam*$^{-1}$.

Table 3. Radio-continuum observations.

Radio Telescope	*Freq* (MHz)	*Beam Size*	*Reference*
MOST	843	$49'' \times 43''$	Whiteoak and Green (1996)
ATCA	1378	$21''$	This study.
Parkes	4850	$4.2'$	Wright et al. (1994)

2.2 ROSAT

ROSAT's Position Sensitive Proportional Counter (PSPC) and High Resolution Imager (HRI) collected 2.7 ksec and 15 ksec observations, respectively, of data for MSH 11–61A in 1993 and 1995. The *ROSAT* archive contain these observations along with HRI observations from 1997 and PSPC observations from 1994.

Details of the *ROSAT* mission can be found in Trümper (1982). Since the counts for the relatively short exposure PSPC image are expected to be low, we did not attempt a detailed spectral analysis. In Fig. 2 we show the 15 ksec HRI *ROSAT* image (energy range 0.5 – 2.4 keV) binned to $5''$ pixels and smoothed for better representation.

The X-ray field contains many sources at other wavelengths (infrared, optical, radio and X-ray) most of which are foreground stars. A SIMBAD search did not reveal any X-ray coincidences with known sources at other wavelengths.

2.3 CO

We also obtained NANTEN CO images of the MSH 11-61A region centered at l=290°, b=–0.5; courtesy of Norikazu Mizuno (Nagoya University). This 4-meter radio telescope was set to the 13CO line at 110 GHz. Installed at the Las Campanas Observatory in Chile, its half power beam width (HPBW) is $2.7'$ at 110 GHz. Its pointing accuracy is about $20''$ based on scanning studies of Jupiter. The front end of this telescope is a 4 K cryogenically cooled Nb SIS mixer receiver (Fukui et al. 1999). The images presented here (see Fig. 5) correspond to velocity channels (2 km s^{-1} steps) ranging from –10 to +39 km s^{-1}.

3. RESULTS and DISCUSSION

Since this SNR is a significantly extended object in our ATCA and MOST images, we used the MIRIAD task IMSTAT to estimate flux densities at 1384 and 843 MHz. To estimate the MSH 11–61A flux density in the 4850 MHz (PMN) image, we fitted a gaussian model using MIRIAD's IMFIT. Results from our analysis are listed in Table 4.

Angular sizes of MSH 11–61A are listed for each frequency. We used major and minor axis dimensions given by IMFIT for the 4850 MHz image. Dimensions for the ATCA and MOST images were found with Karma's *kpvslice*. Values for the 843 MHz image agree with that published by Whiteoak and Green (1996).

Estimates of the spectral index (α) are based on flux densities obtained from corresponding radio-frequencies (see Tables 2 and 4). The spectral index α is defined by the relation $S_\nu \sim \nu^\alpha$, where S_ν is the integrated flux density and ν is frequency. The errors in spectral index ($\Delta\alpha$) have been deduced given the scatter in flux density.

In Fig. 3, we plot flux densities versus respective frequencies of MSH 11–61A. Our calculated spectral index of -0.33 ± 0.07 fits nicely on this graph. We note that the 408 MHz flux density (Shaver and Gross 1970) appears greater than expected which may be the result of measurement errors but inclusion of surrounding Galactic emission may also explain this. Further inspection suggests a turn-over of the spectral index at the mid to low frequencies. Contrary to the X-ray frequencies, it seems most likely that the mechanism of radio-continuum emission in MSH 11–61A is non-thermal.

Table 4. Measured radio-continuum properties.

Frequency (MHz)	1378	843	4850
Beam Size (B_{Size})	$21''$	$49'' \times 43''$	$5'$
Angular Size	$18' \times 13'$	$19' \times 14'$	$11' \times 8.6'$
RMS Noise (mJy)	2.5	1.5	19.3
Flux Density (Jy)	31.5	41.4	22.74
Spectral Index		-0.33 ± 0.07	

=

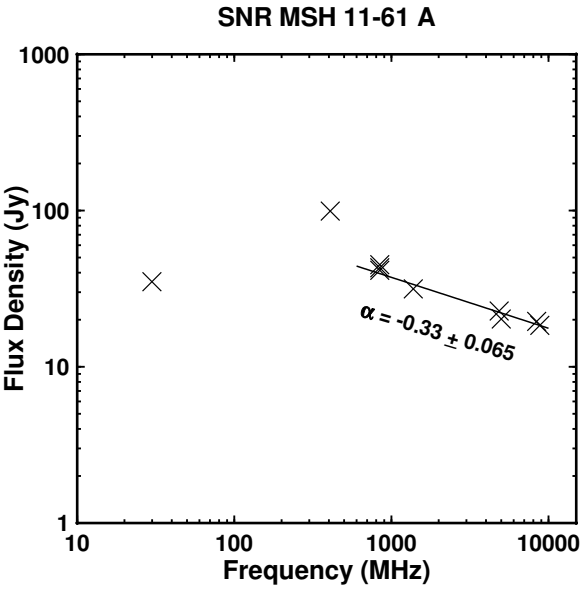

Fig. 3. *Radio spectral index plot (log-log scale) of MSH 11–61A.*

A calculated spectral index image between the 843 MHz and 1378 MHz images was created using MIRIAD's task SMOOTH to bring the 1378 MHz image resolution to that of the 843 MHz image. After applying the task REGRID to the smoothed image, MATHS was used to calculate the spectral index of each pixel not blanked using a 5 σ mask. The map (Fig. 4) ranging from a spectral index of –0.9 to greater than –0.1 (average $\alpha = -0.33$) shows a non-uniform distribution of spectral indices with a flat central region suggestive of a pulsar wind nebula (PWN). Could this be the as yet unidentified neutron star associated with this remnant?

As noted earlier, the morphology of MSH 11–61A has been described differently in the radio and X-ray domains. One can see why this is so in comparison of the ATCA (Fig. 1) and *ROSAT* (Fig. 2) images. The *ROSAT* image is much better resolved than previous X-ray images and demonstrates a center-filled emission that is not uniform in distribution. This possibly makes sense of the Cloudy ISM model discussed by Slane et al. (2002) involving a two-phase ISM with cold clouds embedded in a warmer diffuse intercloud medium. There is also an area of increased X-ray emission centrally although no definite evidence of a stellar core has ever been found and is not suggested by the thermal X-ray nature of MSH 11–61A.

Like the *ROSAT* image, the ATCA image (Fig. 1) of MSH 11–61A is not uniform in nature although areas of increased emission do not correspond exactly to the X-ray image. There appears to be increased brightness near the southwest edge of the object possibly giving rise to the 'shell' description that appears so often in the literature. Equally, central regions also show increased radio flux which could be labeled as centrally filled. Obviously, no simple term can fully describe this object.

The kinematics of molecular clouds in the direction of MSH 11-61A are studied by using the CO images shown in Fig. 5. These images are quite similar to H II region kinematics by Rosado et al. (1996) using the Hα line. The complex nature of foreground and background nebulae are manifested by different velocities seen in projection.

Although our images do not cover the –20 km s^{-1} region, it is possible to see CO emission northeast of the remnant in Fig. 5a at -9 km s^{-1}. This continues to about +1 km s^{-1} seen in Fig. 5f. Emission southwest of MSH 11-61A peaks at about +20 km s^{-1} as shown in Figs. 5o and 5p. Another peak emission from this region is seen at +32 km s^{-1} in Figs. 5u and 5v.

If we adopt the rotation curve given by Brand and Blitz (1993), the distance 7 kpc corresponds to the V_{lsr} ∼7.8 km s^{-1} (see Fig. 5i). Using this information with that given by Rosado et al. (1996) (see discussion in Section 1), we infer that the sharply defined radio emission from the southwest rim of MSH 11-61A (Figs. 1 and 2) may be associated with a molecular cloud between +7 and +23 km s^{-1}. This is consistent with a distance between 7 and 8 kpc.

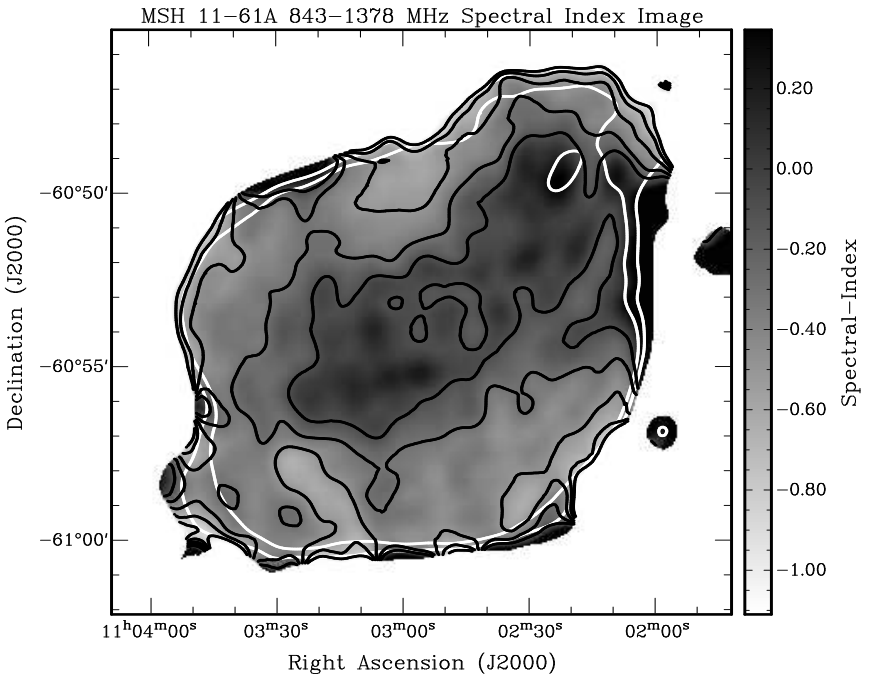

Fig. 4. *843–1378 MHz spectral index image. White MOST (843 MHz) contours at 0.05 and 0.10 Jy beam^{-1} overlay the image with black spectral contours at –0.9, –0.7, –0.5, –0.3 and -0.1 (outside inward).*

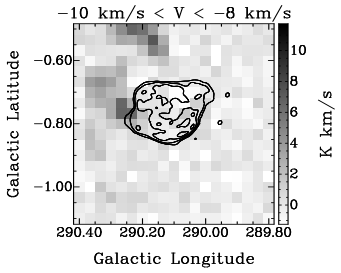

Fig. 5a. V_{lsr}=*–9 km s*$^{-1}$.

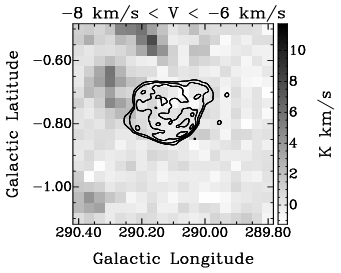

Fig. 5b. V_{lsr}=*–7 km s*$^{-1}$.

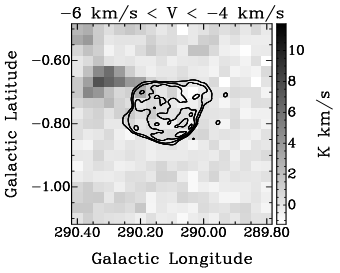

Fig. 5c. V_{lsr}=*–5 km s*$^{-1}$.

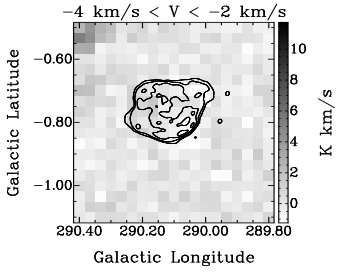

Fig. 5d. V_{lsr}=*–3 km s*$^{-1}$.

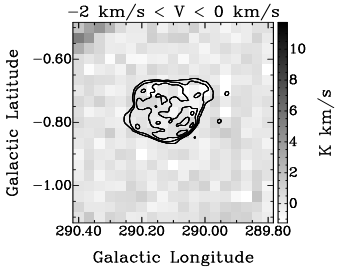

Fig. 5e. V_{lsr}=*–1 km s*$^{-1}$.

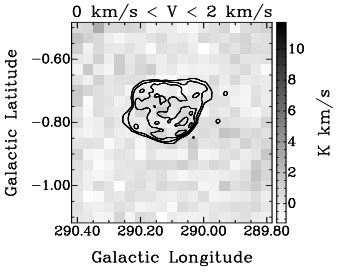

Fig. 5f. V_{lsr}=*+1 km s*$^{-1}$.

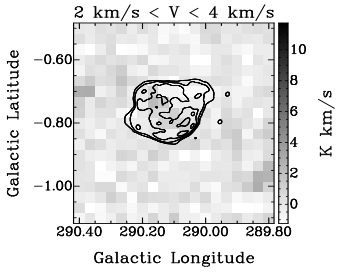

Fig. 5g. V_{lsr}=*+3 km s*$^{-1}$.

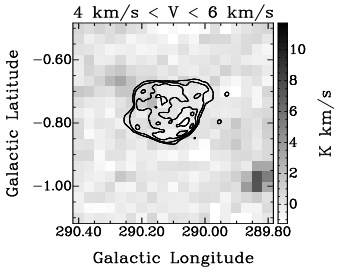

Fig. 5h. V_{lsr}=*+5 km s*$^{-1}$.

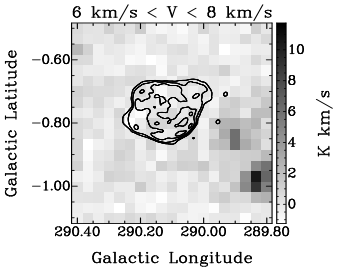

Fig. 5i. V_{lsr}=*+7 km s*$^{-1}$.

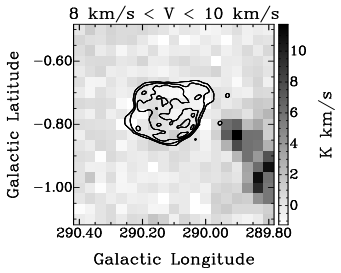

Fig. 5j. V_{lsr}=*+9 km s*$^{-1}$.

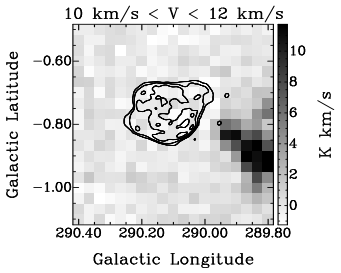

Fig. 5k. V_{lsr}=*+11 km s*$^{-1}$.

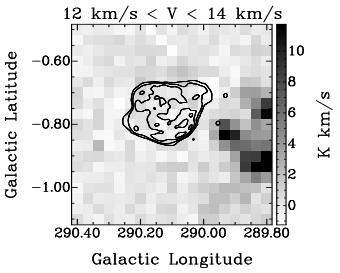

Fig. 5l. V_{lsr}=*+13 km s*$^{-1}$.

Fig. 5. *CO images of MSH 11–61A. Each image correspond to the velocity channels (2 km s*$^{-1}$ *steps). The given* V_{lsr} *includes a range of* ±1 *km s*$^{-1}$*. MOST contours overlay all images (0.05, 0.1, 0.2 and 0.3 Jy beam*$^{-1}$*).*

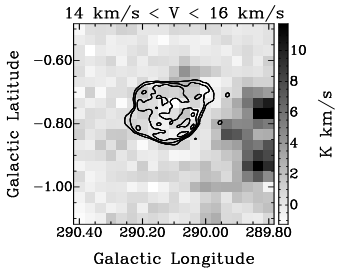

Fig. 5m. *V_{lsr}=+15 km s^{-1}.*

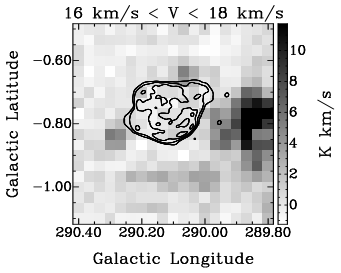

Fig. 5n. *V_{lsr}=+17 km s^{-1}.*

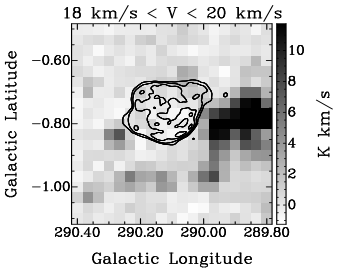

Fig. 5o. *V_{lsr}=+19 km s^{-1}.*

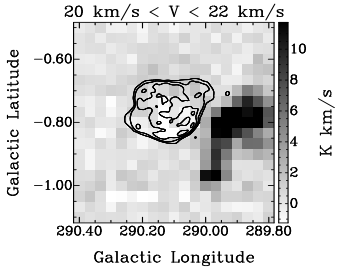

Fig. 5p. *V_{lsr}=+21 km s^{-1}.*

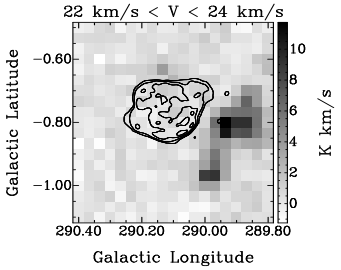

Fig. 5q. *V_{lsr}=+23 km s^{-1}.*

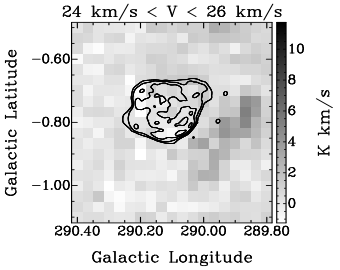

Fig. 5r. *V_{lsr}=+25 km s^{-1}.*

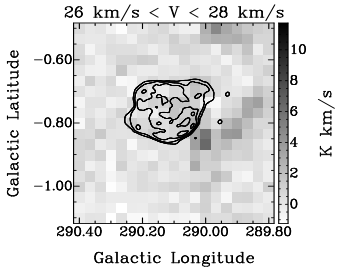

Fig. 5s. *V_{lsr}=+27 km s^{-1}.*

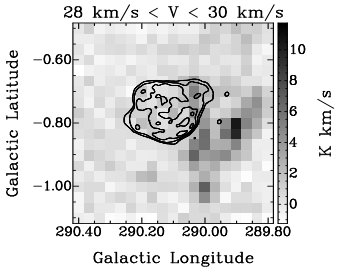

Fig. 5t. *V_{lsr}=+29 km s^{-1}.*

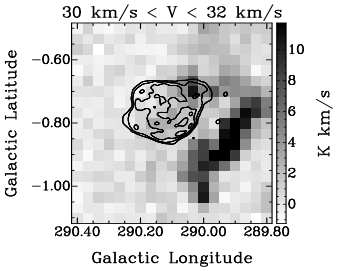

Fig. 5u. *V_{lsr}=+31 km s^{-1}.*

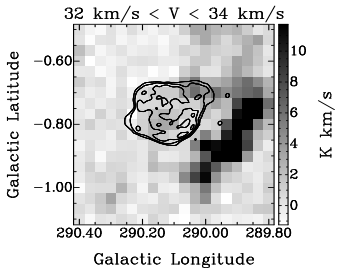

Fig. 5v. *V_{lsr}=+33 km s^{-1}.*

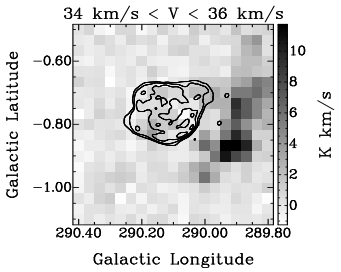

Fig. 5w. *V_{lsr}=+35 km s^{-1}.*

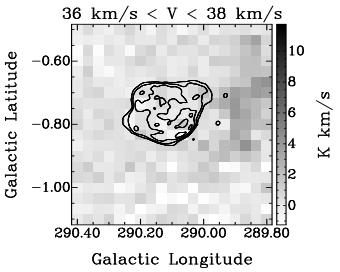

Fig. 5x. *V_{lsr}=+37 km s^{-1}.*

Fig. 5. *(cont.) CO images of MSH 11–61A. Each image correspond to the velocity channels (2 km s^{-1} steps). The given V_{lsr} includes a range of ±1 km s^{-1}. MOST contours overlay all images (0.05, 0.1, 0.2 and 0.3 Jy beam^{-1}).*

4. CONCLUSIONS

We present a new ATCA image of MSH 11–61A at 1378 MHz and re-examine images at 843 and 4850 MHz finding a spectral index of -0.33 ± 0.07, consistent with previous calculations along this portion of the radio-continuum spectrum. A *ROSAT* HRI image of this SNR reveals the difference in morphology between radio and X-ray domains.

A spectral index map of MSH 11–61A suggests that the central region may have a thermal radio component although it is not possible to demonstrate a central massive object. If this remnant was produced by massive star, it may be associated with a dense molecular region seen in CO images suggesting a kinematic distance between 7 and 8 kpc. This is consistent with other distance determinations.

Acknowledgements – We used the Karma/MIRIAD software package developed by the ATNF and the EXSAS/MIDAS software package developed by the MPE. The *ROSAT* project is supported by the German BMBF and the MPG. We thank N. Mizuno for the CO Nanten images and W. Becker for the *ROSAT* X-ray image. We also thank T.G.P. for his keen suggestions and comments.

REFERENCES

Brand, J., Blitz, L.: 1993, *Astron. Astrophys.*, **275**, 67.
Clark, D. H., Caswell, F. L.: 1976, *Mon. Not. R. Astron. Soc.*, **174**, 267.
Cowie, L. L., McKee, C. F.: 1977, *Astrophys. J.*, **211**, 135.
Cox, D. P., Shelton, R. L., Maciejewska, W., Smith, R. K., Plewa, T., Pawl, A., Ròżycka, M.: 1999, *Astrophys. J.*, **524**, 179.
Dickel, J. R.: 1973, *Astrophys. J.*, **15**, L61.
Dickel, J. R., Milne, D. K., Kerr, A. R., Ables, J. G.: 1973, *Aust. J. Phys.*, **26**, 379.
Elliot, K. H., Malin, D. F.: 1979, *Mon. Not. R. Astron. Soc.*, **186**, 45E.
Fukui, Y., Muzuno, N., Yamaguchi, R., et al.: 1999, *Publ. Astron. Soc. Japan*, **51**, 745.
Green, D. A.: 2001, 'A Catalogue of Galactic Supernova Remnants (2001 December version)', Mullard Radio Astronomy Observatory, Cavendish Laboratory, Cambridge, United Kingdom, `http://www.mrao.cam.ac.uk/surveys/snrs/`.
Griffith, M. R., Wright, A. E.: 1993, *Astron. J.*, **105**, 1666.
Jones, B. B., Finlay, E. A.: 1974, *Aust. J. Phys.*, **27**, 687J.
Kaspi, V. M., Bailes, M., Manchester, R. N., Stappers, B.W., Sandhu, J. S., Navarro, J., D'Amico, N.: 1997, *Astrophys. J.*, **485**, 820.
Kesteven, M. J. L.: 1968, *Aust. J. Phys.*, **21**, 739.
Kirshner, R. P., Winkler, P. F.: 1979, *Astrophys. J.*, **227**, 853.
Milne, D. K., Caswell, J. L., Kesteven, M. J., Haynes, R. F., Roger, R. S.: 1989, *Publ. Astron. Soc. Australia*, **8 (2)**, 187.
Milne, D. K., Dickel, J. R.: 1975, *Aust. J. Phys.*, **28**, 209.
Rho, J., Petre, R.: 1998, *Astrophys. J.*, **503**, L167.
Rosado, M., Ambrocio-Cruz, P., Le Coarer, E., Marcelin, M.: 1996, *Astron. Astrophys.*, **315**, 243.
Sault R., Killeen N.: 2003, MIRIAD *users Guide*, Aus. Teles. Nat. Fac. (ATNF), Australia.
Seward, F. D.: 1990, *Astrophys. J. Suppl. Series*, **73**, 781.
Shaver, P. A., Goss, W. M.: 1970, *Aust. J. Phys. Suppl. Series*, **14**, 133.
Slane, P., Smith, R. K., Hughes, J. P., Petre, R.: 2002, *Astrophys. J.*, **564**, 284.
Trümper J.: 1982, *Advances in Space Research*, **2**, 241.
Whiteoak, J. B. Z., Green, A. J.: 1996, *Astron. Astrophys. Suppl. Series*, **118**, 329.
White, R. L., Long, K. S.: 1991, *Astrophys. J.*, **373**, 543.
Wright, A. E., Griffith, M. R., Burke, B. F., Ekers, R. D.: 1994, *Astrophys. J. Suppl. Series*, **91**, 111.

РАДИО ПОСМАТРАЊА ГАЛАКТИЧКОГ ОСТАТКА СУПЕРНОВЕ MSH 11-61A

M. D. Filipović[1], J. L. Payne[2] and P. A. Jones[3]

[1] *University of Western Sydney, Locked Bag 1797, Penrith South DC NSW 1797, Australia*

[2] *Centre for Astronomy, James Cook University, Townsville QLD 4811, Australia*

[3] *Australia Telescope National Facility, CSIRO, P.O. Box 76, Epping NSW 1710, Australia*

UDK 524.354–735–77
Оригинални научни рад

У овој студији представљамо истраживања високе резолуције у (континуалном) делу радио спектра галактичког остатка супернове MSH 11-61A. Користили смо и посматрања из других делова спектра (област икс-зрака и CO) да бисмо боље проучили морфологију и кинематику овог необичног остатка супернове. Континуални радио спектрални индекс смо проценили на -0.33 ± 0.07, базирано на нашим мерењима радио флукса. Такође, примећујемо да овај остатак супернове има обрнут радио спектар на нижим радио фреквенцијама (29.9 – 843 MHz). Дијаметар MSH 11-61A процењујемо на $12.5'$ са додатним проширењем северзапад од $4'$ са сваке стране. Упадљива антикорелација између икс-зрачних и радио посматрања потврђује ранију класификацију овог остатка супернове као морфолошки мешовиту класу. Наша CO посматрања потврђују раније процењену удаљеност до овог остатка супернове од око 7 kpc (Rosado et al. 1996).